Experimental elucidation of vacancy complexes associated with hydrogen ion-induced splitting of bulk GaN

O. Moutanabbir,* R. Scholz, and U. Gösele†
Max Planck Institute of Microstructure Physics, Weinberg 2, Halle (Saale) 06120, Germany

A. Guittoum, M. Jungmann, M. Butterling, and R. Krause-Rehberg
Martin-Luther-University Halle-Wittenberg, Friedemann-Bach-Platz 6, Halle (Saale) 06108, Germany

W. Anwand
Forschungszentrum Dresden-Rossendorf, P.O. Box 510119, 01314 Dresden, Germany

W. Egger and P. Sperr
Universität der Bundeswehr, Werner-Heisenberg-Weg 39, 85579 Neubiberg, Germany
(Received 29 October 2009; revised manuscript received 1 February 2010; published 5 March 2010)

We present a detailed study of the thermal evolution of H ion-induced vacancy related complexes and voids in bulk GaN implanted under ion-cut conditions. By using transmission electron microscopy, we found that the damage band in as-implanted GaN is decorated with a high density of nanobubbles of ~1–2 nm in diameter. Variable energy Doppler broadening spectroscopy showed that this band contains vacancy clusters and voids. In addition to vacancy clusters, the presence of V_{Ga}, V_{Ga}-H_2, and $V_{Ga}V_N$ complexes was evidenced by pulsed low-energy positron lifetime spectroscopy. Subtle changes upon annealing in these vacancy complexes were also investigated. As a general trend, a growth in open-volume defects is detected in parallel to an increase in both size and density of nanobubbles. The observed vacancy complexes appear to be stable during annealing. However, for temperatures above 450 °C, unusually large lifetimes were measured. These lifetimes are attributed to the formation of positronium in GaN. Since the formation of positronium is not possible in a dense semiconductor, our finding demonstrates the presence of sufficiently large open-volume defects in this temperature range. Based on the Tao-Eldrup model, the average lattice opening during thermal annealing was quantified. We found that a void diameter of 0.4 nm is induced by annealing at 600 °C. The role of these complexes in the subsurface microcracking is discussed.

DOI: 10.1103/PhysRevB.81.115205 PACS number(s): 61.72.−y, 61.80.−x, 68.37.−d, 81.05.Ea

I. INTRODUCTION

Blue GaN-based laser diodes emitting a coherent and narrow spectral line at 450 nm open up new applications in optoelectronic data storage, visual information, medical devices, and biophotonics.[1] These diodes are based on high-quality In-rich InGaN quantum wells grown by metal-organic vapor-phase epitaxy on GaN substrates with a low defect density.[2] To meet this crystalline quality requirement, bulk or free-standing (fs) GaN substrates are used in the fabrication of blue laser diodes instead of the relatively highly defective GaN epilayers grown on foreign substrates. High-crystalline quality fs-GaN wafers are usually obtained by hydride vapor-phase epitaxy growth of thick GaN layers on sapphire and subsequent separation from sapphire substrates.[3] Beyond the blue laser-based applications, the availability of these fs-GaN substrates can potentially impact on other devices such as power devices and ultrahigh brightness light-emitting diodes (LEDs).[4] However, the current cost of these fs-GaN wafers remains too high to allow a large scale production of these new devices. Therefore, in order to compete with the alternative technologies (e.g., SiC), an important decline in fs-GaN cost is needed.

One of the possible strategies to reduce the cost would be the splitting of several thin layers from a single fs-GaN wafer (donor wafer) and their transfer onto appropriate handle wafers. In principle, this can be achieved by using the ion-cut process, commercially known as smart cut.[5,6] In this process, hydrogen (H) and/or helium (He) energetic ions are implanted (under well-controlled conditions) into a donor wafer. After implantation, the implanted wafer is bonded to a handle wafer. During annealing at intermediate temperatures, the interaction of the implanted species with the radiation damage acts as an atomic scalpel producing extended internal surfaces. This leads to the splitting and transfer of a thin layer with a thickness equivalent to the implantation depth. Note, however, that layer transfer can only take place if the bonded interface donor/handle remains stable during thermal annealing. Ion cut is currently used in the fabrication of silicon-on-insulator and germanium-on-insulator wafers.[5,7] These successful applications of the ion-cut process have led since mid-1990s to a sharp increase in the experimental and theoretical studies of H (and He) interactions with implantation-induced defects and their thermal behavior in order to decipher the fundamental mechanisms responsible of the layer splitting.[8–10] A few works have also reported on this phenomenon in some conventional compound semiconductors.[11–13] Techniques such as vibrational spectroscopies,[14–19] transmission electron microscopy,[10,20] Rutherford backscattering spectrometry in the channeling mode,[21–23] x-ray diffraction,[24] and positron annihilation spectroscopy[22,25] improved greatly our understanding of the

microscopic mechanisms of the ion-cut process (particularly in Si). These studies have demonstrated the critical role of H-vacancy (H-*V*) complexes and damage-generated stress in the formation of nanoscopic platelets and voids immediately after implantation. Thermal annealing was found to induce an increase in open-volume defects parallel to a rearrangement in H-*V* complexes characterized by a collapse of multivacancy complexes and persistence (or even increase) in highly passivated monovacancies. Despite the absence of conclusive evidence, it is generally assumed that the formation and trapping of H_2 molecules trigger the observed microstructural transformations. Annealing above a critical temperature leads to a relaxation of the internal strain by subsurface microcracking.

In contrast to the case of Si, only a few studies of ion-implantation-induced GaN layer splitting were reported so far.[26–29] In those studies, phenomenological aspects of H blistering of GaN were addressed exclusively letting unexplored the atomic processes and the underlying physics. Recently, in order to explore the basic mechanisms involved in the ion-induced splitting of GaN, we employed several complementary experimental techniques to study the microstructure produced by H ions and its thermal evolution. This has led to the identification of some critical structural transformations leading to the layer splitting of bulk GaN.[30,31] However, for a better understanding of the microscopic mechanisms, the role of point-defect and H-defect complexes should be investigated in details. In this paper, we elucidate the nature of vacancy complexes and voids involved in H ion-induced splitting of GaN. For this purpose, we used variable-energy Doppler broadening spectroscopy (VEDBS) in order to probe open-volume defects and their thermoevolution. Pulsed low-energy positron lifetime spectroscopy (PLEPLS) was employed to qualitatively characterize H ion-induced vacancy complexes and to observe their subtle changes during the thermally activated splitting of GaN thin layer. The associated morphology of the implanted region was studied systematically by using transmission electron microscopy.

II. EXPERIMENTAL DETAILS

Our experiments were carried out using LED quality ~ 300 μm thick 2 in. double side polished fs-GaN wafers. The wafers were subject to room-temperature implantation with 50 keV H ions corresponding to H mean depth of ~ 320 nm, as measured by elastic recoil detection.[30] For its part, atomic displacement field peaks at a shallower depth around ~ 285 nm estimated from ion-channeling analysis.[30] The wafers were implanted with a fluence in the range of $(0.5-3.0)\times 10^{17}$ H/cm^2. After implantation, fs-GaN wafers were annealed in N_2 atmosphere at different temperatures ranging from 100 to 600 °C. After standard cross-section preparation including thinning by ion milling, pieces from the wafers, as implanted or annealed, were observed by transverse-section electron microscopy (XTEM) using a Philips CM 20T machine operated at 200 kV. XTEM images were taken off-focus in order to highlight some implantation-induced nanoscopic features. Positron annihilation experiments were performed on similar samples.

Depth-profiled Doppler broadening measurements were carried out using the variable-energy positron beam at the Research Center Dresden-Rossendorf. Positrons were produced by a 10 mCi ^{22}Na source assembled in transmission with a 1 μm monocrystalline tungsten moderator, transported in a magnetic guidance system. A beam having a diameter of 4 mm and an intensity of $\approx 10^2 \beta^+/\mathrm{s}$ was used in the analysis. The samples were mounted in an UHV chamber at room temperature. The γ annihilation spectrum was recorded with a high-purity Ge detector having an energy resolution of $\approx(1.09\pm 0.01)$ keV at 511 keV. The data were processed with a digitally stabilized multichannel-analyzer system. The Doppler broadening of the 511 keV γ-ray peak was measured as a function of the incident positron energy E in the range of 0.03–35 keV. At each energy E, a spectrum with approximately 5×10^5 total counts was collected in the 511 keV annihilation line. In VEDBS measurements, the Doppler broadening of the 511 keV annihilation line is characterized by the so-called S parameter, which is defined as the ratio of the counts in a central region of the 511 keV annihilation photopeak to those in the whole area of this line. In this experiment, the S parameter is normalized to the S value measured for bulk GaN in the as-received state.

PLEPLS measurements were conducted at the positron beam facility NEPOMUC at the Munich Research Reactor FRM II.[32,33] This system produces a sharp positron pulse of 150 ps in full width at the half maximum with high intensity and low background in between the pulses at the location of the sample. To preserve the same pulse shape at all implantation energies, only the final sharp pulses are accelerated to the desired implantation energy. After acceleration, the positrons pass the field-free Faraday cage until they reach the specimen, in which they annihilate. One of the annihilation quanta is registered by the detector (BaF_2 scintillator coupled to fast photomultiplier) below the sample station and the time between implantation and annihilation is measured to accumulate the lifetime spectrum. In our experiments, the positron beam with energy varying from 0.5 to 18 keV was used. At a fixed implanted positron energy, data were collected for more than 10^6 annihilation events at room temperature. The lifetime spectrum of positrons, $D(t)$, is given by

$$D(t) = \sum_i I_i/\tau_i \exp[-t/\tau_i],$$

where τ_i and I_i represent the positron lifetimes and their corresponding intensities, respectively. The observed spectra were analyzed using POSWIN software[34] in which the resolution function was a sum of three Gaussian distributions. Generally, the experimental results are presented in terms of the average positron lifetime τ_{av} defined as

$$\tau_{av} = \sum_i I_i \tau_i.$$

The average lifetime is statistically a rather accurate parameter because it does not depend much on the spectra decomposition.

III. RESULTS AND DISCUSSION

After annealing for 5 min at 600 °C, only GaN samples implanted with a fluence $\geq 2.6\times10^{17}$ H^+/cm^2 display a large density of dome-shaped blisters indicative of subsurface microcracking. Implantation below this critical fluence does not produce any blistering even after annealing for long durations at temperatures as high as 900 °C. This agrees well with earlier observations.[26] This very high critical fluence is one of the most striking differences between GaN and other semiconductors in which a few 10^{16} H^+/cm^2 is sufficient to induce the exfoliation. Supported by studies of damage buildup in GaN implanted with different ions (e.g., C, Si, Au, etc.),[35] several authors have postulated that the high critical fluence is attributed to a very efficient dynamic annealing of point defects in GaN.[26–29] This explanation stands in sharp contrast to the blistering behavior of GaN implanted with H at low temperature. In fact, no change in the critical fluence is observed when the implantation is carried out at liquid-nitrogen temperature at which the dynamic annealing of point defects is significantly reduced.[26] In contrast, low-temperature implantation was found to increase the thermal budget indicating that a larger accumulation of defects makes actually the blistering even harder to trigger.[26] Therefore, it appears to be inaccurate to attribute the high critical fluence to a pronounced dynamic annihilation of the implantation-induced point defects. The extrapolation of data obtained with other ions to the H case can be fraught with uncertainty. In fact, one has to consider the chemical reactivity of H and the stabilizing effect of dangling bond passivation in addressing defect dynamic annealing and damage buildup in H-implanted semiconductors.[36] Alternatively, the intrinsic mechanical properties as well as the nature of H-induced defects may be critical in determining the fluence of H ions needed to cleave GaN. Another peculiarity of GaN is the absence of the synergistic effect upon successive implantations with He and H ions in both orders, which was efficient in reducing the critical fluence and thermal budget in other semiconductors (see, e.g., Refs. 19 and 37, and references therein). Intriguingly, we found that the implantation of He alone requires the same critical fluence as H. Also, this critical fluence does not vary when highly *p*-doped GaN is used instead of undoped GaN. Note that in Si, for instance, the critical fluence decreases greatly for highly *p*-doped substrates.[38–40] These observations suggest that the phenomenon of ion-induced exfoliation may be fundamentally different in GaN as compared to the well-studied semiconductors. Consequently, it is worthwhile to elucidate the fundamental aspects of H exfoliation of GaN. Here, we focus our investigation on undoped substrates implanted with H ions at the critical fluence of 2.6×10^{17} H^+/cm^2.

Figure 1 displays a XTEM image of as-implanted GaN. We note that H ion implantation induces a broad damage band extending over a 300-nm-thick layer starting about 200 nm below the surface. No extended defects are observed at the implanted fluence. Instead, a high density of nanoscopic bright spots of ~1–2 nm in diameter is detected. The change in their contrast during focus variation suggests that they are voidlike structures (nanobubbles). A drastic decrease in their density is observed beyond a depth of ~280 nm.

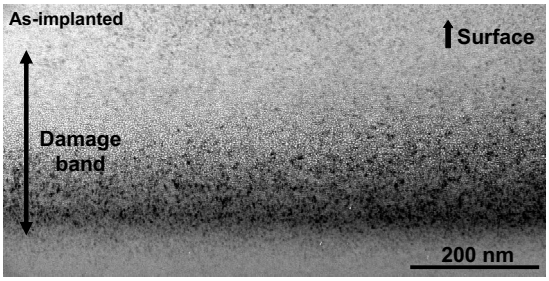

FIG. 1. XTEM image of H-implanted free-standing GaN for an implantation energy of 50 keV and a fluence of 2.6×10^{17} cm^{-2}. H ion-induced nanobubbles are visible as 1–2 nm bright spots.

During the implantation of energetic H ions into GaN several physical and chemical processes take place leading to a variety of damage-related structures including point defects in both sublattices, H-defect complexes, point-defect clusters, and free hydrogen. A first attempt to experimentally identify H-defect complexes in H-implanted GaN was published by Weinstein *et al.*[41] They found that the IR absorption spectrum of as-implanted GaN displays two main vibrational bands centered at 3139.5 and 3023.1 cm^{-1} (as measured at liquid-He temperature). These modes were attributed to H trapped in N dangling bond defects near a Ga vacancy (V_{Ga}). The band at the highest frequency is attributed to a V_{Ga}-H_4 mode while the band at the lowest frequency is associated to V_{Ga}-H_n containing fewer H atoms (i.e., $n\leq3$). However, the data obtained by Weinstein *et al.*[41] cannot be directly extended to our case because the fluence implanted in their case is approximately two orders of magnitude lower than the critical fluence of H exfoliation of GaN. Our preliminary IR data (not shown) indicate that a large fraction of H is trapped in higher frequency modes $k>3140$ cm^{-1} (beyond V_{Ga}-H_4 frequency), which we tentatively attributed to N-H stretch modes in the internal surfaces of implantation-induced nanobubbles.[31] No Ga-H (or V_N-H) related mode was detected in our samples. From this, it is reasonable to assume that the observed nanobubbles (Fig. 1) are the result of H stabilization of V_{Ga} clusters.

As described above, large extended internal surfaces develop upon annealing of H-implanted GaN. Figure 2 shows a typical XTEM image of H-implanted GaN after annealing at 600 °C for 5 min. We note that annealing has led to the cleavage of ~340-nm-thick GaN layer. The thickness of this layer is close to the H ion mean range (~320 nm), which is suggestive of a preferential microcracking near the H concentration peak. However, unlike the case of H implantation at excessively high fluences,[42] annealing here does not lead to the formation of large (~20 nm) faceted cavities.

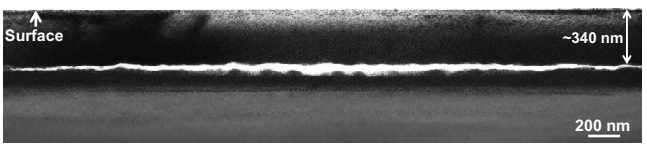

FIG. 2. XTEM image of H-implanted GaN substrate implanted under the conditions described in Fig. 1 and annealed at 600 °C for 5 min.

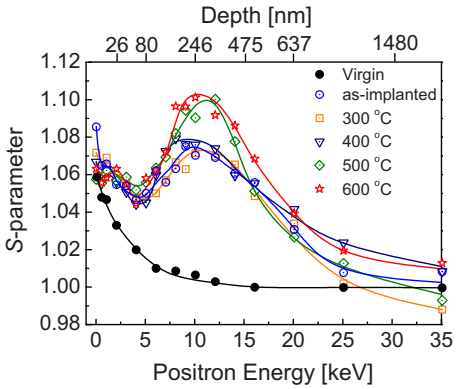

FIG. 3. (Color online) Thermoevolution of the normalized S parameter of H-implanted GaN samples as a function of incident positron energy. For comparison, the spectrum recorded from bulk GaN is also shown.

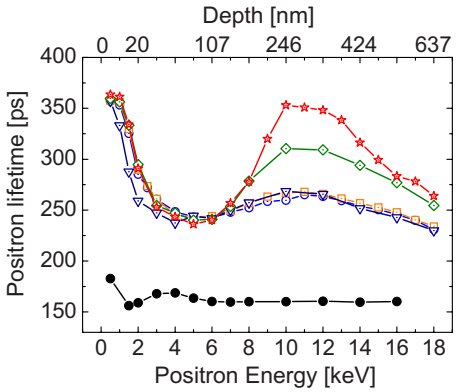

FIG. 4. (Color online) The evolution of the average positron lifetime as a function of the positron energy for the virgin, as-implanted, and annealed GaN samples. The symbols are the same as in Fig. 3.

The evolution of vacancy-related complexes and voids is investigated next. Since positron annihilation is insensitive to large open volumes, we limit our analysis to samples annealed for 2 min corresponding to the subcritical regime. Figure 3 shows the "shape" or S parameter as a function of incident positron energy (S-E curve) for the unimplanted, proton-implanted, and annealed GaN samples at different temperatures. The top horizontal axis shows the mean implantation depth of the positrons. The S values are normalized to $S=1.0$ for defect-free bulk GaN ($S_N=S/S_b$) in the bulk (at maximum positron energy), and any increase in S_N above this value is indicative of open-volume defects. Defined in this way, the S_N parameter can be used as an approximate gauge of the type of defect. For example, S_N for monovacancies is 1.030, S_N for divacancies is 1.034–1.044, small vacancy clusters are expected to have 1.05–1.07, and for voids S_N is 1.10–1.14.[43,44]

From Fig. 3, it can be seen that for the unimplanted sample, the S_N parameter decreases gradually from the surface state to the bulk state with increasing energy, and becomes constant at $E>10$ keV. At low positron energies (0–2 keV), the positron penetration depth is so low that the positrons can diffuse back to the surface. The higher S parameter values, observed for all samples, near the surface are attributed to an enhanced annihilation possibly due to surface contamination. After proton implantation and annealing, we can see, in addition to the annihilation at the surface, the presence of annihilations in two different regions: the region around 10 keV, where S_N exhibits the maximum values and the defect-free region beyond the implanted zone (>500 nm).

In the implanted region the maximum defect density is located at a depth of about 250 nm close to the displacement peak measured by ion channeling.[30] Before and after annealing, the S_N values are greater than 1.0 indicating the presence of open-volume defects. Moreover, for this depth of 250 nm, all S_N values are higher than the specific value of 1.055, which is typically associated to $V_{Ga}V_N$ complex.[45] Nevertheless, due to the complexity of the ion-induced microstructure, the contribution from other defects cannot be excluded. Hence, we can conclude that in this region the majority of defects generated after implantation and also after annealing are larger than monovacancies. Similar observations were recently reported by Tuomisto *et al.*[46] for 100 keV H ion-implanted GaN at a fluence of 5×10^{17} cm^{-2}. Immediately after implantation, the maximum value of S_N is 1.071, which indicates that the implantation has produced vacancy clusters. Their depth profile coincides well with the observed nanobubbles (Fig. 1). After annealing at 300 and 400 °C, the S_N values are practically the same as for the as-implanted state, which means that the defects present are stable against annealing in this temperature range.

Interestingly, for GaN samples annealed at 500 and 600 °C, the S_N values are equal to 1.09 and 1.101, respectively. This suggests that larger voids grow after annealing above 500 °C. Similar voids were also observed by Fan *et al.*[43] in GaN films implanted with Al^+ immediately after implantation.

In Fig. 4, we present the evolution of the average lifetime vs positron energy for the virgin GaN, as-implanted and annealed samples. The first remark that we can make is the overall similarity in the behavior of the average lifetime and S_N parameter with positron energy. From Fig. 4, it can be clearly seen that for the virgin sample, the average positron lifetime shows the bulk lifetime equal to 162 ps at high positron implantation depth.[47] This indicates the absence of positron traps at least for a depth greater than 100 nm. After implantation and as a result of positron trapping into open-volume defects, the average lifetime becomes much higher than the bulk one. After implantation and also after annealing, the average lifetime at the surface (depth below 100 nm) is high due to the low electron density. The same behavior is also observed for S parameter. Moreover, in the range of 200–500 nm, we can clearly see the presence of a maximum as a result of defect generation by H implantation. This maximum increases with increasing annealing temperature especially for 500 and 600 °C.

After implantation and annealing, the lifetime spectra were fitted with three lifetime components by using the POSWIN software.[34] Figure 5 displays the evolution of the three lifetimes τ_1, τ_2, τ_3 with their intensities. The decomposition of the lifetime spectra is also presented in Table I for

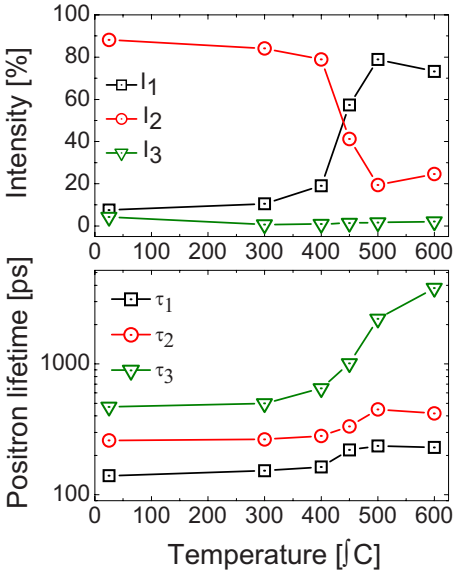

FIG. 5. (Color online) The decomposition of the lifetime spectra for the virgin, as-implanted, and annealed GaN samples extracted at a positron energy of 10 keV.

the positron energy of 10 keV corresponding to a depth of about 246 nm. It appears that for the as-implanted and annealed samples at 300 and 400 °C, the first lifetime τ_1 is smaller than the one in bulk GaN. According to recent *ab initio* calculations,[45] this component may be related to the presence of a Ga vacancy defect containing two hydrogen atoms V_{Ga}-H_2. Indeed, hydrogen pushes the positron density out from the vacancy leading to a shorter lifetime. Note, that for Ga vacancy-related defects, the typical lifetime is $\tau(V_{Ga})=235$ ps.[48] After annealing at 450, 500, and 600 °C, the values of τ_1 are equal to 220 ps, 236 ps, and 230 ps, respectively. These lifetimes are not far from the typical value of Ga vacancy. Hence, we can conclude that for these temperatures, the defects corresponding to this lifetime are monovacancies.

For the second lifetime τ_2, a clear increase from 260 ps for the as-implanted sample to 332 ps for the annealing temperature of 450 °C is observed. Moreover, the values of τ_2 are longer than the positron lifetime for V_{Ga} (235 ps) previously reported. It can be concluded that up to a temperature

TABLE I. Decomposed lifetimes of the as-implanted and annealed GaN samples measured at a positron energy of 10 keV.

	Lifetimes and intensities of the components		
Sample	τ_1/I_1 (ps/%)	τ_2/I_2 (ps/%)	τ_3/I_3 (ps/%)
As implanted	140/7.6	260/88.2	470/4.2
Annealed at 300 °C	152/10.49	265/84.11	500/0.74
Annealed at 400 °C	160/19	282/78.85	650/0.95
Annealed at 450 °C	220/57.36	332/41.22	1008/1.42
Annealed at 500 °C	236/78.92	449/19.44	2215/1.64
Annealed at 600 °C	230/73.22	418/24.65	3811/2.13

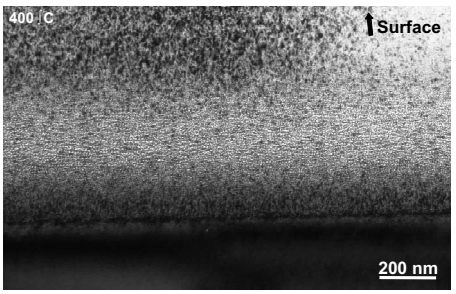

FIG. 6. XTEM image of H-implanted GaN substrate under the conditions described in Fig. 1 and annealed at 400 °C for 2 min.

of 450 °C, the defects present are divacancies ($V_{Ga}V_N$) or at least have an open volume similar to this defect. It is important to note that the existence of divacancies was also reported by Uedono *et al.*[49] in the case of implanted and annealed GaN samples. After annealing at 500 and 600 °C, the values of τ_2 equal 449 and 418 ps and are so large that they cannot arise from either monovacancies or divacancies. The lifetimes of 449 and 418 ps are indicative of the presence of vacancy clusters.[50,51] This result is in accordance with that obtained from S parameter measurements described above (Fig. 3).

For the third lifetime τ_3, the values of 470, 500, and 600 ps indicate also the presence of vacancy clusters up to 400 °C. However, for the annealing temperature of 450, 500, and 600 °C, the values of τ_3 are equal to 1, 2.2, and 3.8 ns. These values are larger than the longest lifetime which can be expected for positron annihilation in a solid. In analogy with an early study of voids in a-Si,[52] these unusually long lifetimes can only be attributed to the formation of positronium within the open-volume regions in the annealed ($T \geq 450$ °C) H-implanted GaN. Based on the Tao-Eldrup model,[53] one can estimate the average open-volume corresponding to these long lifetimes. We found that the lifetimes of 1 ns, 2.2 ns, and 3.8 ns correspond to a void diameter of about 0.2 nm, 0.3 nm and 0.4 nm, respectively. Intriguingly, the formation of the positronium was not observed in the as-implanted GaN despite the presence of sufficiently large voidlike structures (Fig. 1).

Let us now turn to XTEM data. Figure 6 displays a XTEM micrograph of H-implanted GaN annealed at 400 °C for 2 min. No significant qualitative change is detected in the damage band compared to the as-implanted state (Fig. 1). The same nanobubbles are still observable. However, their density appears to increase upon annealing at 400 °C. Interestingly, neither Doppler broadening (Fig. 3) nor lifetime (Fig. 4) measurements show a difference between as-implanted and 400 °C annealed samples. Therefore, it can be inferred that these nanobubbles are somehow *invisible* to positrons. Two factors can explain this discrepancy: the lack of open volume due to H trapping within these nanobubbles (i.e., the nanobubbles are actually filled with H) and an overall positive charge of the complex. The diameter of these nanobubbles increases significantly (up to ~7 nm) upon annealing at 600 °C (Fig. 7). Again, such a drastic increase in nanobubble size is not visible in the positron data (Fig. 4) where the largest wall spacing is found to be 0.4 nm at the

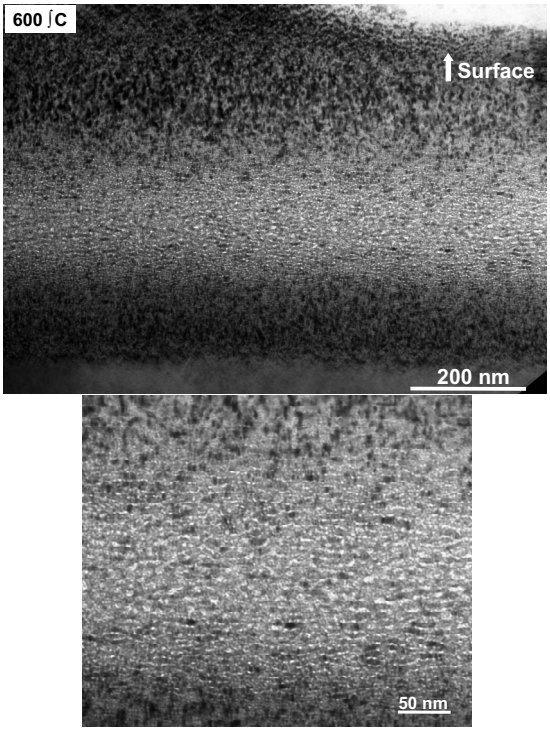

FIG. 7. (Top) XTEM image of H-implanted GaN substrate under the conditions described in Fig. 1 and annealed at 600 °C for 2 min. (Bottom) High magnification XTEM image of the damage band.

highest temperature of 600 °C, too small compared to the size of open-volume defects observable in Fig. 7. Based on this *conflict* between positron data and XTEM, one can distinguish between two sets of open-volume defects: (1) those visible for positrons and invisible by XTEM (e.g., too small) and (2) those visible by XTEM and invisible for positrons (too large, filled, or positively charged complexes).

It is interesting to note that for the as-implanted and annealed GaN samples, the Doppler measurements reveals only two vacancy-type defects in the as-implanted and annealed GaN, namely, vacancy clusters and voids, whereas the decomposition of the lifetime spectra of the same samples suggests the presence of other types of defects (V_{Ga}, V_{Ga}-H_2, and $V_{Ga}V_N$). While it is hard to describe the role of each defect in H implantation-induced layer splitting of GaN, it is plausible to attribute a physical role (internal pressure and strain buildup) to nanobubbles and a chemical role (bonds weakening and breakage) to H-*V* complexes. The strain builds up during annealing likely due to the trapping of free H available in GaN lattice by nanobubbles as well as to interstitial clusters as demonstrated by high-resolution x-ray diffraction.[31] The strain starts to relax around 450 °C,[31] which corresponds to the beginning of lattice opening reaching a spacing of 0.2 nm. Annealing above this temperature increases the spacing to reach 0.3 nm and 0.4 nm for 500 °C and 600 °C, respectively. A pronounced relaxation was indeed detected in this temperature range.[31] The formation of this subnanometer spacing can be at the origin of subsurface microcracking.

IV. CONCLUSION

To conclude, we have studied the thermoevolution of defects in H implanted and annealed free-standing GaN under ion-cut conditions. XTEM data showed that the damage band in as-implanted GaN is decorated with a high density of nanobubbles of ~1–2 nm in diameter. These nanobubbles persist and their density and diameter increase during annealing. The decomposition of the lifetime spectra of as-implanted and annealed samples up to a temperature of 450 °C resulted in the detection of two vacancy-related defects: divacancies (260–282 ps) and vacancy clusters (470–650 ps). With increasing temperature, we have noted, in addition to the already mentioned defects, the presence of another kind of vacancy defects, namely, monovacancies (220–236 ps) and a long lifetime which is attributed to positronium. From the values of positronium lifetimes equal to 1, 2.2 and 3.8 ns, it was possible to estimate the corresponding average void diameter according to the Tao-Eldrup model to be in the 0.2–0.4 nm range. The formation of these nanoscopic open-volume defects takes place in the subcritical regime preceding GaN layer splitting. This leads us to consider the observed voids as embryos of the subsurface microcracking leading to thin layer splitting.

ACKNOWLEDGMENTS

This work was supported by the German Ministry of Education and Research (BMBF) under CrysGaN project (Contract No. 01BU0624).

*moutanab@mpi-halle.mpg.de
†Deceased.

[1] S. Lutgen and M. Schmitt, Optik & Photonik **2**, 37 (2009).
[2] H. Morkoç, *Handbook of Nitride Semiconductors and Devices*, Materials Properties, Physics and Growth Vol. 1 (Wiley-VCH, Weinheim, 2008).
[3] S. S. Park, I.-W. Park, and S. H. Park, Jpn. J. Appl. Phys., Part 2 **39**, L1141 (2000).
[4] Bulk GaN Market 2009 (market research report).
[5] M. Bruel, Electron. Lett. **31**, 1201 (1995).
[6] O. Moutanabbir, S. Senz, R. Scholz, S. Christiansen, A. Avramescu, U. Strauss, and U. Gösele, Electrochem. Solid-State Lett. **12**, H105 (2009).
[7] C. Deguet, L. Sanchez, T. Akatsu, F. Allibert, J. Dechamp, F. Madeira, F. Mazen, A. Tauzin, V. Loup, C. Richtarch, D. Mercier, T. Signamarcheix, F. Letertre, B. Depuydt, and N. Kernevez, Electron. Lett. **42**, 415 (2006); Y.-L. Chao, R. Scholz, M. Reiche, U. Gösele, and J. C. S. Woo, Jpn. J. Appl. Phys., Part 2 **45**, 8565 (2006).
[8] For a review on silicon see: B. Terreault, Phys. Status Solidi A

204, 2129 (2007).
[9] J. M. Zahler, A. Fontcuberta i Morral, M. J. Griggs, H. A. Atwater, and Y. J. Chabal, Phys. Rev. B **75**, 035309 (2007).
[10] M.-L. David, L. Pizzagalli, F. Pailloux, and J. F. Barbot, Phys. Rev. Lett. **102**, 155504 (2009).
[11] A. Fontcuberta i Morral, J. M. Zahler, M. J. Griggs, H. A. Atwater, and Y. J. Chabal, Phys. Rev. B **72**, 085219 (2005).
[12] P. Chen, Z. Di, M. Nastasi, E. Bruno, M. G. Grimaldi, N. D. Theodore, and S. S. Lau, Appl. Phys. Lett. **92**, 202107 (2008).
[13] S. Hayashi, M. Goorsky, A. Noori, and D. Bruno, J. Electrochem. Soc. **153**, G1011 (2006).
[14] M. K. Weldon, V. E. Marsico, Y. J. Chabal, A. Agarwal, D. J. Eaglesham, J. Sapjeta, W. L. Brown, D. C. Jacobson, Y. Caudano, S. B. Christman, and E. E. Chaban, J. Vac. Sci. Technol. B **15**, 1065 (1997).
[15] M. K. Weldon, M. Collot, Y. J. Chabal, V. C. Venezia, A. Agarwal, T. E. Haynes, D. J. Eaglesham, S. B. Christman, and E. E. Chaban, Appl. Phys. Lett. **73**, 3721 (1998).
[16] Y. J. Chabal, M. K. Weldon, Y. Caudano, B. B. Stefanov, and K. Raghavachari, Physica B **273-274**, 152 (1999).
[17] O. Moutanabbir and B. Terreault, J. Chem. Phys. **121**, 7973 (2004).
[18] J. Weber, T. Fisher, E. Hieckmann, M. Hiller, and E. V. Lavrov, J. Phys.: Condens. Matter **17**, S2303 (2005).
[19] O. Moutanabbir and B. Terreault, Appl. Phys. Lett. **86**, 051906 (2005).
[20] P. Nguyen, I. Cayrefourcq, K. K. Bourdelle, A. Boussagol, E. Guiot, N. Ben Mohamed, N. Sousbie, and T. Akatsu, J. Appl. Phys. **97**, 083527 (2005).
[21] T. Höchbauer, A. Misra, M. Nastasi, and J. W. Mayer, J. Appl. Phys. **92**, 2335 (2002).
[22] O. Moutanabbir, B. Terreault, M. Chicoine, F. Schiettekatte, and P. J. Simpson, Phys. Rev. B **75**, 075201 (2007).
[23] Z. F. Di, Y. Q. Wang, M. Nastasi, L. Shao, J. K. Lee, and N. D. Theodore, Appl. Phys. Lett. **93**, 104103 (2008).
[24] M. Nastasi, T. Höchbauer, J.-K. Lee, J. P. Hirth, M. Ridgway, and T. Lafford, Appl. Phys. Lett. **86**, 154102 (2005); J.-K. Lee, Y. Lin, Q. X. Jia, T. Höchbauer, H. S. Jung, L. Shao, A. Misra, and M. Nastasi, *ibid.* **89**, 101901 (2006); N. Sousbie, L. Capello, J. Eymery, F. Rieutord, and C. Lagahé, J. Appl. Phys. **99**, 103509 (2006).
[25] P. J. Simpson, A. P. Knights, M. Chicoine, K. Dudeck, O. Moutanabbir, S. Ruffel, F. Schiettekatte, and B. Terreault, Appl. Surf. Sci. **255**, 63 (2008).
[26] S. O. Kucheyev, J. S. Williams, C. Jagadish, J. Zou, and G. Li, J. Appl. Phys. **91**, 3928 (2002).
[27] I. Radu, R. Singh, R. Scholz, U. Gösele, S. Christiansen, G. Brüderl, C. Eichler, and V. Härle, Appl. Phys. Lett. **89**, 031912 (2006).
[28] R. Singh, I. Radu, U. Gösele, and S. H. Christiansen, Phys. Status Solidi C **3**, 1754 (2006).
[29] H. J. Woo, H. W. Choi, W. Hong, J. H. Park, and C. H. Eum, Surf. Coat. Technol. **203**, 2375 (2009).
[30] O. Moutanabbir, R. Scholz, S. Senz, U. Gösele, M. Chicoine, F. Schiettekatte, F. Süßkraut, and R. Krause-Rehberg, Appl. Phys. Lett. **93**, 031916 (2008).
[31] O. Moutanabbir, Y. J. Chabal, M. Chicoine, S. Christiansen, R. Krause-Rehberg, F. Schiettekatte, R. Scholz, O. Seitz, S. Senz, F. Süßkraut, and U. Gösele, Nucl. Instrum. Methods Phys. Res. B **267**, 1264 (2009).
[32] W. Egger, P. Sperr, G. Kögel, and G. Dollinger, Phys. Status Solidi C **4**, 3969 (2007).
[33] C. Hugenschmidt, T. Brunner, S. Legl, J. Mayer, C. Piochacz, M. Stadlbauer, and K. Schreckenbach, Phys. Status Solidi C **4**, 3947 (2007).
[34] D. Bochert, Diploma thesis, Universität der Bundeswehr, 2004.
[35] S. O. Kucheyev, J. S. Williams, and S. J. Pearson, Mater. Sci. Eng. R. **33**, 51 (2001).
[36] O. Moutanabbir, R. Scholz, U. Gösele, and B. Terreault, Phys. Rev. B **79**, 233202 (2009).
[37] I. Radu, I. Szafraniak, R. Scholz, M. Alexe, and U. Gösele, J. Appl. Phys. **94**, 7820 (2003).
[38] Q.-Y. Tong, R. Scholz, U. Gösele, T.-H. Lee, L.-J. Huang, Y.-L. Chao, and T. Y. Tan, Appl. Phys. Lett. **72**, 49 (1998).
[39] J. K. Lee, T. Höchbauer, R. D. Averitt, and M. Nastasi, Appl. Phys. Lett. **83**, 3042 (2003).
[40] N. Desrosiers, A. Giguère, O. Moutanabbir, and B. Terreault, Appl. Phys. Lett. **87**, 231908 (2005).
[41] M. G. Weinstein, C. Y. Song, M. Stavola, S. J. Pearton, R. G. Wilson, R. J. Shul, K. P. Killeen, and M. J. Ludowise, Appl. Phys. Lett. **72**, 1703 (1998).
[42] C. H. Seager, S. M. Myers, G. A. Peterson, J. Han, and T. Headley, J. Appl. Phys. **85**, 2568 (1999).
[43] H. Yi-Fan, C. D. Beling, and S. Fung, Chin. Phys. Lett. **22**, 1214 (2005).
[44] P. J. Schultz and K. G. Lynn, Rev. Mod. Phys. **60**, 701 (1988).
[45] S. Hautakangas, I. Makkonen, V. Ranki, M. J. Puska, K. Saarinen, X. Xu, and D. C. Look, Phys. Rev. B **73**, 193301 (2006).
[46] F. Tuomisto, Appl. Surf. Sci. **255**, 54 (2008).
[47] K. Saarinen, S. Hautakangas, and F. Tuomisto, Phys. Scr. **T126**, 105 (2006).
[48] K. Saarinen, T. Laine, S. Kuisma, J. Nissilä, P. Hautojärvi, L. Dobrzynski, J. M. Baranowski, K. Pakula, R. Stepniewski, M. Wojdak, A. Wysmolek, T. Susuki, M. Leszczynski, I. Grzegory, and S. Porows, Phys. Rev. Lett. **79**, 3030 (1997).
[49] A. Uedono, K. Ito, H. Nakamori, K. Mori, Y. Nakano, T. Kachi, S. Ishibashi, T. Ohdaira, and R. Suzuki, J. Appl. Phys. **102**, 084505 (2007).
[50] S. Hautakangas, K. Saarinen, L. Liszkay, J. A. Freitas, Jr., and R. L. Henry, Phys. Rev. B **72**, 165303 (2005).
[51] S. Hautakangas, J. Oila, M. Alatalo, and K. Saarinen, Phys. Rev. Lett. **90**, 137402 (2003).
[52] Y. J. He, M. Hasegawa, R. Lee, S. Berko, D. Adler, and A.-L. Jung, Phys. Rev. B **33**, 5924 (1986).
[53] S. J. Tao, J. Chem. Phys. **56**, 5499 (1972); M. Eldrup, D. Lightbody, and J. N. Sherwood, Chem. Phys. **63**, 51 (1981).